Received: 14 December 2018 | Accepted: 15 April 2019

DOI: 10.1002/hyp.13469

RESEARCH ARTICLE

WILEY

Impact of the spatial variability of daily precipitation on hydrological projections: A comparison of GCM- and RCM-driven cases in the Han River basin, Korea

Moon-Hwan Lee[1] | Eun-Soon Im[1,2] | Deg-Hyo Bae[3]

[1] Department of Civil and Environmental Engineering, The Hong Kong University of Science and Technology, Hong Kong

[2] Division of Environment and Sustainability, The Hong Kong University of Science and Technology, Hong Kong

[3] Department of Civil and Environmental Engineering, Sejong University, South Korea

Correspondence
Eun-Soon Im, Department of Civil and Environmental Engineering, The Hong Kong University of Science and Technology, Academic Building 3594, Clear Water Bay, Kowloon, Hong Kong.
Email: ceim@ust.hk

Deg-Hyo Bae, Department of Civil and Environmental Engineering, Sejong University, 209 Neungdong-ro, Gwangjin-gu, Seoul 05006, South Korea.
Email: dhbae@sejong.ac.kr

Funding information
Ministry of Environment, Grant/Award Number: RE201901084

Abstract

In this study, we investigate the impact of the spatial variability of daily precipitation on hydrological projections based on a comparative assessment of streamflow simulations driven by a global climate model (GCM) and two regional climate models (RCMs). A total of 12 different climate input datasets, that is, the raw and bias-corrected GCM and raw and bias-corrected two RCMs for the reference and future periods, are fed to a semidistributed hydrological model to assess whether the bias correction using quantile mapping and dynamical downscaling using RCMs can improve streamflow simulation in the Han River basin, Korea. A statistical analysis of the daily precipitation demonstrates that the precipitation simulated by the GCM fails to capture the large variability of the observed daily precipitation, in which the spatial autocorrelation decreases sharply within a relatively short distance. However, the spatial variability of precipitation simulated by the two RCMs shows better agreement with the observations. After applying bias correction to the raw GCM and raw RCMs outputs, only a slight change is observed in the spatial variability, whereas an improvement is observed in the precipitation intensity. Intensified precipitation but with the same spatial variability of the raw output from the bias-corrected GCM does not improve the heterogeneous runoff distributions, which in turn regulate unrealistically high peak downstream streamflow. GCM-simulated precipitation with a large bias correction that is necessary to compensate for the poor performance in present climate simulation appears to distort streamflow patterns in the future projection, which leads to misleading projections of climate change impacts on hydrological extremes.

KEYWORDS

climate change, dynamical downscaling, hydrological projection, spatial variability of precipitation

1 | INTRODUCTION

The factors affecting a streamflow hydrograph can be divided into watershed structures (e.g., size, shape, slope, and roughness), precipitation characteristics (e.g., amount, intensity, and duration of precipitation), and antecedent conditions (e.g., soil moisture; Singh, 1987). Although watershed structures are prescribed at a time initially for running a hydrological model, precipitation data should be regularly updated because precipitation initiates the hydrological processes and affects the antecedent conditions of soil moisture. Therefore, precipitation characteristics that vary considerably over space and time can be the determining factors that shape the behaviour of streamflow

simulations in hydrological modelling. In particular, the spatial variability of precipitation has a dominant influence on the rainfall–runoff response (Cristiano, ten Veldhuis, & van de Giesen, 2017; Merz & Bardossy, 1998). Many studies have demonstrated that the accuracy of the shape and peak timing of a streamflow simulation depends largely on the spatial variability of the precipitation data used as input to run hydrological models (Beven & Hornberger, 1982; Henn et al., 2018; Kokkonen, Koivusalo, Karvonen, & Croke, 2004; Smith et al., 2004). Although a particular basin receives the same amount of total precipitation, the distribution of precipitation and the location of the maximum precipitation nearest to or farthest from the catchment outlet can result in significantly different hydrographs in terms of the magnitude and timing of peak flow.

Given the scientific consensus that enhanced greenhouse gas (GHG) emissions can modulate the intensity and frequency of daily precipitation (Giorgi, Coppola, & Raffaele, 2014; IPCC, 2013; Trenberth, Dai, Rasmussen, & Parsons, 2003), it is reasonable to expect that changes in precipitation characteristics will subsequently lead to changes in both the mean streamflow and hydrological extremes (e.g., flood and drought). A significant body of research has attempted to quantify the effect of precipitation change on regional hydrology under a changing climate (Chang & Jung, 2010; Coppola, Raffaele, & Giorgi, 2018; Jung, Bae, & Lee, 2013; Zhang, Karthikeyan, Bai, & Wang, 2017). When pursuing this subject, it is challenging to obtain reliable future climate data, particularly at fine spatial and temporal scales. Despite the large uncertainty and scaling gap, future climate projections generated using global climate models (GCMs) are the only information that can account for the complex and nonlinear processes of climate systems in response to enhanced GHG emission forcings. To alleviate the obvious problems embedded in GCM projections, downscaling and/or bias correction are generally considered to be standard procedures, although further levels of uncertainty are added to climate data (Lee & Bae, 2018). The pros and cons of statistical and dynamical downscaling methods are still a subject of debate, and a clear conclusion to support the superiority of one method over the other has not been obtained. Although there are comparative studies to appeal the scepticism about the computationally expensive technique of dynamical downscaling using regional climate models (RCMs; e.g., Ahmed et al., 2013; Ngai, Tangang, & Juneng, 2017), a number of studies have demonstrated the added values of dynamically downscaled simulations in capturing detailed climate features in particular regions (e.g., Lee, Lu, Im, & Bae, 2019; Torma, Giorgi, & Coppola, 2015; Tselioudis, Douvisa, & Zerefos, 2012). However, when linking downscaled climate projections to the impact assessment sector, the usage of statistically postprocessed GCMs tends to be more dominant than the usage of dynamically downscaled GCMs using RCMs. For example, many hydrological impact assessments have applied spatial disaggregation and statistical bias correction to GCM projections (Eden, Widmann, Maraun, & Vrac, 2014; Shrestha, Schnorbus, Werner, & Zwiers, 2014). These studies consistently argue that the incorporation of dynamical downscaling as an intermediate step may not lead to considerable differences compared with the results that are obtained by directly applying simple spatial disaggregation and statistical bias correction to GCMs. If a spatially disaggregated GCM with bias correction could be an alternative that is sufficiently substituted for a dynamically downscaled GCM with bias correction, it would be desirable to increase the number of GCM ensemble members rather than to perform dynamical downscaling to improve the reliability of future climate projections. However, the utilization of dynamical downscaling seems to be evaluated in a fragmented way, with most of the focus on temporally and spatially averaged patterns. In this regard, this study revisits the question of whether disaggregated GCM and RCM results show apparent differences when linking to hydrological simulations.

Arguably, the most important improvement that would be expected from the utilization of RCMs over GCMs is that RCMs can better resolve the heterogeneity of complex geographical settings that mainly determine the region-specific climatology over a target area. GCMs typically have a horizontal resolution of more than 100 km and may have difficulty in accurately parameterizing the fine-scale physical processes at regional to local scales (Im & Eltahir, 2018). Previous studies have consistently shown that this difficulty is particularly true for climate simulations over the Korean Peninsula, where the necessity of applying RCMs is highly recognized due to the complicated geographical features of the area (Ahn et al., 2016; Im, Kwon, Ahn, & Giorgi, 2007; Oh et al., 2016; Suh et al., 2016). For example, most GCM grid systems fail to capture realistic mountain slopes and land–sea distributions in Korea, which is directly associated with their poor performance in simulating mesoscale convective systems and orographically induced circulations that in turn shape precipitation patterns. Nevertheless, bias correction using statistical methods (e.g., quantile mapping [QM] and linear scaling) seems to rescue GCM projections, which enables them to feed hydrological models because the statistical fitting of raw outputs to historical observations can effectively eliminate the systematic bias during the reference period. Therefore, the performances of bias-corrected GCMs and bias-corrected RCMs appear to be independent of the performance of the raw output, at least in terms of long-term averaged climatology (Lee, Lu, et al., 2019). However, as Lee, Lu, et al. (2019) demonstrated, the correction factor calculated on a monthly basis may not be effective in correcting the daily variation of output, especially when the correction factors are large. More importantly, a large bias correction factor used to compensate for the poor performance of historical climate simulations can potentially induce misleading or exaggerated interpretations of future extremes when the same correction factor is applied to future climate projections.

In this study, we explore the behaviour of daily precipitation in terms of spatial variability and its impact on hydrological projections. Because precipitation is characterized by its highly discrete nature and distinct variation, state-of-the-art GCMs and RCMs still show a limited ability to reproduce the detailed characteristics of daily precipitation. Therefore, it is imperative to understand how the deficiency in simulated precipitation is transferred into hydrological processes, which will provide insights into the model-dependent implications of this common deficiency in hydrological modelling studies for climate change impact assessment. First, the analysis

focuses on the comparisons of the spatial variability of daily precipitation derived from two RCMs, which are RegCM4 (Regional Climate Model Version 4, Giorgi et al., 2012, hereafter referred to as RegCM) and WRF3.4 (Weather Research and Forecasting Version 3.4, Skamarock et al., 2008, hereafter referred to as WRF), and their driving GCM (Hadley Centre Global Environmental Model Version 2-Atmosphere–Ocean, Collins et al., 2011, hereafter referred to as HadGEM). All projections used in this study were generated to establish Korean national standard climate change scenarios. Both raw outputs and bias-corrected outputs using QM from the GCM and two RCMs are compared to identify whether the GCM and two RCMs show different performances in simulating the spatial variability of daily precipitation and how effectively bias correction improves the performance of the raw outputs. To quantitatively measure the ability of climate models to capture the spatial similarity or dissimilarity of daily precipitation as a function of distance, we introduce two useful statistical methods, namely, the Pearson correlation coefficient (CC; Berndtsson, 1988) and variogram (Cressie, 1993). With a deeper understanding of the characteristics of daily precipitation, hydrological modelling with SWAT (Soil and Water Assessment Tool, Arnold, Srinivasan, Muttiah, & Williams, 1998) is then performed over the Han River basin in Korea using the 12 different climate input datasets, which include the raw and bias-corrected GCM and raw and bias-corrected two RCMs outputs for the reference and future periods. The assessment of how differently the GCM and RCM simulate the spatial variability of daily precipitation with and without statistical bias correction and the effect on hydrological simulations will facilitate the proper use of dynamically downscaled climate information. These results will directly aid the hydrological modelling community in employing the climate simulations that are most suitable for their research.

2 | DATA AND METHODOLOGY

2.1 | Study area and observation

Figure 1a shows the elevation map of South Korea derived from a 30-m digital elevation model. The geographical features of South Korea are characterized by a narrow peninsula with complicated mountainous terrain. Within the grid system employed in HadGEM, all of South Korea and the surrounding ocean are covered by 15 grid points. Therefore, when HadGEM is simply disaggregated, the climate information over South Korea is generated based on these 15 values regardless of how disaggregated the grids are into a fine mesh. It is difficult to expect that disaggregated GCM values can represent detailed characteristics of climatology at regional to local levels.

Hydrological modelling using SWAT is targeted at the Han River basin, which is located in the central Korean Peninsula covering the latitudes 36°30′–38°55′ and longitudes 126°24′–129°02′. The Han River is the second longest river in South Korea and is largely divided into the South Han River and the North Han River. The convergence of the South and North Han Rivers forms the inflows to the Paldang Dam, and the Soyanggang and Chungju multipurpose dams located in the upstream basin of the Paldang Dam affect the flow regulation at the inlet of the Paldang Dam, which is a major water source for the Seoul metropolitan area. To run the spatially semidistributed hydrological model, that is, SWAT, the Han River basin is subdivided into 20 midsized basins, as depicted by the grey lines in Figure 1b. The climate variables from in situ station observations and gridded simulations are converted to values in each subbasin using the Thiessen weighting technique to feed SWAT.

To validate the daily precipitation characteristics and calculate the correction factors applied to the GCM and RCM simulations over

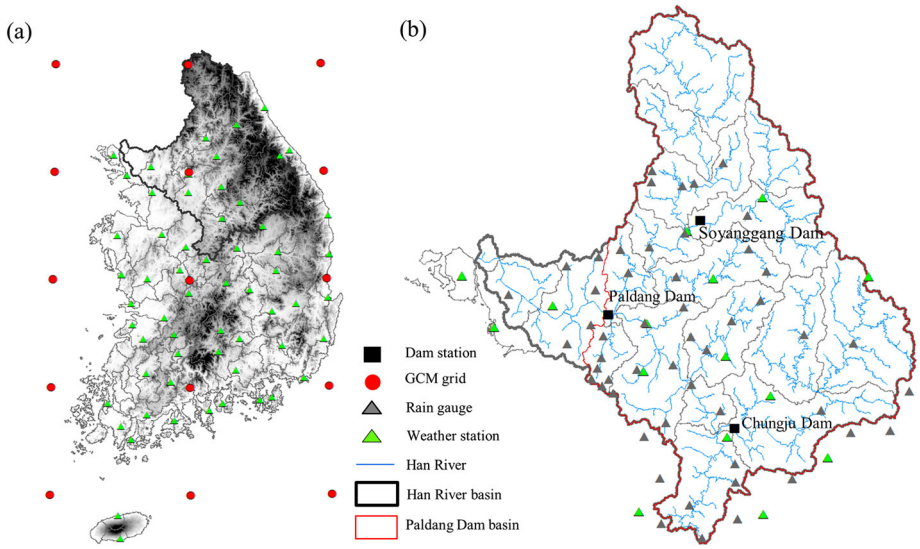

FIGURE 1 Study area. An elevation map of South Korea derived from a 30-m digital elevation model (a) and the Han River basin (b). The red dots in (a) indicate the grid points of HadGEM around the Korean Peninsula. The green triangles in (a) and (b) indicate the weather station of South Korea, and the black triangles in (b) indicate the rain gauges around the Han River. The blue lines in (b) indicate the tributaries of the Han River, and the black squares in (b) indicate the locations of the Paldang, Chungju, and Soyanggang Dams. The yellow regions in (b) indicate the Paldang Dam basins

South Korea, daily precipitation at 60 in situ observational stations (Figure 1a) maintained by the Korean Meteorological Administration are used for the period 1981–2005. Focusing on the Han River basin, daily precipitation at 52 rain gauges maintained by the Korean Ministry of Land, Infrastructure, and Transportation are also used in addition to 15 in situ station observations. Therefore, precipitation observations are collected at a total of 67 locations over the Han River basin (Figure 1b).

2.2 | Climate change projections

The GCM projections are simulated using HadGEM for the historical (1981–2005) and future (2076–2100) periods. Future projections are forced by the representative concentration pathway (RCP8.5) that is equivalent to the business-as-usual emission scenario. HadGEM has a horizontal resolution of 1.75° (longitude) × 1.25° (latitude) and shows reasonable skill in simulating the present climate over East Asia including South Korea (Baek et al., 2013). For fine-scale climate information over South Korea, HadGEM projections are dynamically downscaled using two different RCMs, namely, RegCM and WRF. The domain of both RCMs covers Northeast Asian in the centre of the Korean Peninsula (37.5°N and 127.5°E) with a horizontal resolution of 12.5 km. More detailed descriptions of RegCM and WRF and their basic performance can be found in Oh and Suh (2018) and Im, Ahn, and Jo (2015), respectively. HadGEM projections were generated within the framework of the Coupled Model Intercomparison Project phase 5 (CMIP5; Taylor, Stouffer, & Meehl, 2012), and its downscaled projections focusing on the Korean Peninsula have played an important role in assessing future climate change at the national standard level in South Korea (KMA, 2015).

Because systematic biases are caused by imperfect model dynamics and physics and are inherited from the uncertainties of the initial and boundary conditions, bias correction is a required step not only for GCM outputs but also for RCM outputs when they are used to run hydrological models (Dosio & Paruolo, 2011; Lee, Im, & Bae, 2019; Maurer & Pierce, 2014). There are several bias correction methods, such as linear scaling, variance scaling, and QM. In this study, we apply the QM method to remove the systematic biases of the raw outputs of both the GCM (e.g., HadGEM) and two RCMs (e.g., RegCM and WRF). Because most existing bias correction methods do not apply a theoretical adjustment to the spatial variability of daily precipitation (Vrac & Friederichs, 2015), the selection of other bias correction methods should not introduce a significant difference with the results presented in this study, which is verified by comparing results with the linear scaling results. Only a marginal difference arises from applying linear scaling and QM in terms of the spatial variability (not shown). The QM method fits the cumulative distribution function of a raw output to the observed cumulative distribution function. The QM method is widely used for the bias correction of climate model simulations on a daily scale because this method can adjust not only the mean and variance of climatology but also the daily distribution characteristics. In particular, QM method can efficiently alleviate a well-known problem of climate models, that is, the excessive occurrence of light precipitation using a certain threshold. The threshold, which corresponds to no precipitation (dry day), is calculated from the cumulative probability of observed precipitation, and that threshold is then applied to the simulated distribution to determine the probability of no precipitation. The gamma distribution for precipitation and the Gaussian distribution for temperature are used to estimate the probability distribution functions. It is well recognized that the gamma distribution for precipitation and the Gaussian distribution for temperature are appropriate distributions for applying QM (Lafon, Dadson, Buys, & Prudhomme, 2013; Teng et al., 2015; Teutschbein & Seibert, 2012). Although correction factors are calculated on a monthly basis, the correction factor in a particular month is uniformly applied to all daily data within that month. If the simulated quantity has a larger bias against the observed quantity, the correction factor becomes larger accordingly. Therefore, although bias-corrected patterns on a monthly time-scale derived from historical simulations appear to perfectly match the observed patterns regardless of the performance of the raw simulations, the magnitudes of the applied correction factors are different in accordance with the performances of the raw simulations. Because bias correction is performed under the assumption of stationarity such that bias patterns do not change with time, a large bias correction factor due to poor performance in a present-day climate simulation may disturb future change signals when the same factor is applied to future climate projections. The technical details of the QM method can be found in Lee, Lu, et al. (2019).

In summary, a total of 12 different climate simulations are used for the analysis and to drive the hydrological model in this study: raw HadGEM, RegCM, and WRF outputs for historical and future periods as well as bias-corrected HadGEM, RegCM, and WRF outputs for historical and future periods. For simplicity, raw (bias-corrected) outputs of HadGEM, RegCM, and WRF are denoted as HAD_RAW (HAD_QM), REG_RAW (REG_QM), and WRF_RAW (WRF_QM), respectively.

2.3 | SWAT model

To simulate streamflow in the Han River basin, this study uses a SWAT model, which is a physically based semidistributed hydrological model, to consider the spatial complexity of watershed characteristics as well as climate. This model was developed by the Agricultural Research Service of the United States Department of Agriculture and has been widely applied to analyse and assess the climate change impacts on surface hydrology (Bae, Jung, & Lettenmaier, 2011; Zhou et al., 2013). In this model, a basin is divided into multiple subbasins, which are further subdivided into hydrologic response units that consist of homogeneous land use and soil characteristics (Arnold et al., 1998). Hydrological processes are calculated based on the water balance equation from each hydrologic response unit in a subbasin. The flows are summed in a subbasin and are routed through channels to the basin outlet. Whereas channel routing is simulated using the

Muskingum method (Cunge, 1969), the potential evapotranspiration is calculated using the Penman–Monteith method. More detailed descriptions of the model are given by Arnold et al. (1998).

We set up the SWAT model with 109 midbasins for South Korea, which is the same as that used in the study by Jung et al. (2013), but this study focuses on only the Han River basin (20 midbasins in Figure 1b). To run the SWAT model, daily meteorological variables, such as precipitation, maximum and minimum temperature, solar radiation, relative humidity, and wind speed, are required as input data. We collect the meteorological data (including daily precipitation) at 15 in situ stations and additional daily precipitation data at 52 rain gauges. All of the data are then interpolated by the Thiessen weighing technique to the 20 midbasins. The basin characteristics are represented using geographic information system (GIS) digital databases that include a 30-m digital elevation model, soils, vegetation types, river networks, and land cover, which are provided by the water management information system of Korea. To calibrate the hydrological model parameters, reliable long-term natural flow data are required. Although there are many streamflow gauging stations in the river basins of South Korea, they are significantly influenced by upstream dam operation. Therefore, Jung et al. (2013) used the regionalization method in which the model parameters of ungauged basins are regionalized from the calibrated parameters of the gauged basins. For the regionalization, the parameters of the SWAT model were calibrated at six multipurpose dam sites and the 109 midbasins were categorized into one of six groups, which are the six dam basins based on geophysical characteristics: catchment area, mean altitude, mean slope, ratio of forest, water content at saturation, field capacity, and wilting point of soil. The six different parameter sets were applied to the six basin groups. To validate the performance of SWAT in simulating streamflow, the experiment feeding the observed meteorological data is performed prior to the experiments feeding the model-based simulation data. This experiment enables comparisons of the simulated streamflow with the measured dam inflow. Figure 2 presents the simulated streamflows and measured dam inflow at the inlets to the Chungju, Soyanggang, and Paldang Dams for the period 2001–2005. In general, the simulated flows are in qualitatively and quantitatively good agreement with the measured dam inflows and capture the phase and magnitude in low and high flows. Although there are some discrepancies in the period with low flows, this error may partly be due to measurement uncertainty and dam operation. Because the dam inflow is indirectly measured by the changes in water level of the dams, the accuracy during low flows is rather limited when the change in water level is not large enough, which is partly responsible for the very large fluctuations in the measured low flows at the Chungju and Soyanggang Dams. Moreover, the measured dam inflows at the Paldang Dam are systematically higher than the simulated flows during the low

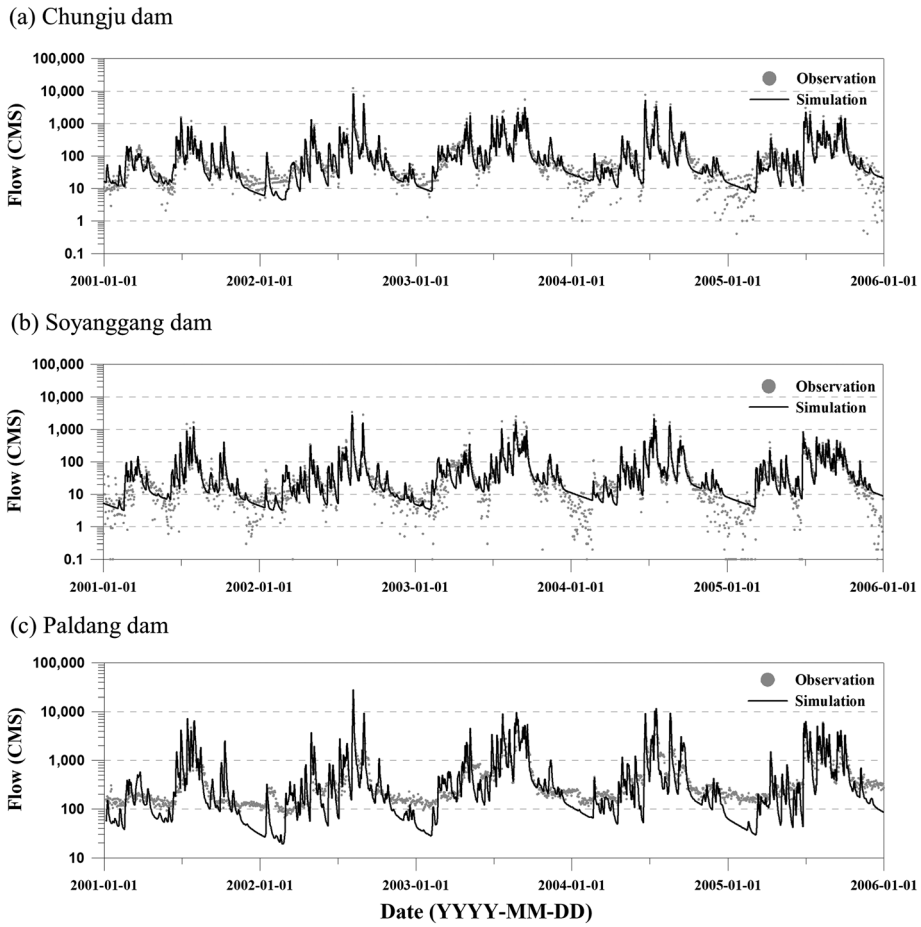

FIGURE 2 Time series of streamflows (2001–2005) in three dam basins: Chungju Dam (a), Soyanggang Dam (b), and Paldang Dam (c). The solid lines represent the streamflows estimated by the hydrological model (SWAT), and the grey dots indicate the measured dam inflow

flow period because the flows at the Paldang Dam are artificially maintained to prevent a base streamflow from lowering below approximately 100 m^3/s, with the aid of the dam operation at the Chungju and Soyanggang Dams, which are the uppermost dams in the South Han River and North Han River, respectively. Therefore, it is regarded that the performance of SWAT is reasonable for analysing the hydrological response (e.g., streamflow) to meteorological conditions (e.g., precipitation) over our target region.

2.4 | CC and variogram

The Pearson CC and variogram are used to quantitatively assess the spatial variability of precipitation. The CC is a measure of linear dependency between a pair of random variables, and it has been widely used to characterize the complex spatial structure of precipitation patterns (Berndtsson, 1988; Habib, Krajewski, & Ciach, 2001). This study applies the CC to analyse the linear dependency of interstations. The CC ($r(X,Y)$) can be estimated by Equation (1) and derived from N station pairs (X,Y):

$$\frac{r(X,\ Y) = \overline{XY} - \overline{XY}}{\sqrt{\left(\overline{X^2} - \overline{X}^2\right)\left(\overline{Y^2} - \overline{Y}^2\right)},} \tag{1}$$

where the overbars indicate average values over the sample of size N.

In addition to CC, we also use a variogram to estimate the temporal coherence of daily precipitation between station pairs as a function of distance between them (Baigorria, Jones, & O'Brien, 2007; Ly, Charles, & Degre, 2011; van de Beek, Leijnse, Torfs, & Uijlenhoet, 2011). In general, the variance of the differences between the values at two locations is calculated as a function of both the direction and distance. However, the assumption that the variable is isotropic enables the variogram to be calculated only as a function of the distance (Xu et al., 2016). In this study, we assume that daily precipitation is isotropic and stationary (Cressie, 1993; van de Beek et al., 2011), and accordingly, the empirical variogram ($\widehat{\gamma}(h)$) is calculated as half of the variance between paired values ($Z(s_i)$,$Z(s_i+h)$) at distance h as follows:

$$\widehat{\gamma}(h) = \frac{1}{2N(h)}\sum_{i=1}^{N(h)}(Z(s_i) - Z(s_i + h))^2, \tag{2}$$

where $N(h)$ is the number of pairs of data points at distance h apart.

An appropriate theoretical model is then fitted to the empirical variogram, and the three measures (e.g., nugget, sill, and range) that characterize the empirical variogram are determined by weighted least squares between two distributions (Cressie, 1985; see Figure 5). The spherical model ($\gamma(h)$), which is widely used to approximate empirical variograms (Merino, Jones, Stooksbury, & Hubbard, 2001; van de Beek et al., 2011), is fitted to the empirical variogram calculated using daily precipitation in this study.

$$\gamma(h) = \begin{cases} C_0 + C_1\left(\frac{3}{2}\frac{h}{C_2} - \frac{1}{2}\left(\frac{h}{C_2}\right)^3\right), & \text{if } h \le C_2 \\ C_0 + C_1, & \text{if } h > C_2 \end{cases}. \tag{3}$$

Here, C_0 is the nugget (the variogram at zero distance), C_1 is the sill (the maximum value of the fitted theoretical variogram model) and C_2 is the range (distance at which data pairs are completely decorrelated). Because of its small value, the nugget was assumed to be negligible in this study. The variance of paired data (e.g., daily precipitation at two locations in this study) increases gradually until it reaches its maximum at a certain distance between two locations whose variables are no longer spatially correlated. The maximum variance is the sill, and the corresponding distance is the range. Because the magnitude of the variance is roughly proportional to the squared precipitation intensity, the large sill values are indicative of intense precipitation events. Moreover, the range decreases as the spatial variability of precipitation becomes larger.

3 | RESULTS

3.1 | Spatial variability of daily precipitation

We begin our analysis by comparing the precipitation derived from different climate models in terms of their performance in simulating the spatial variability over South Korea using 60 in situ stations (Figure 1a); then we focus on the detailed characteristics of the Han River basin. Figure 3 presents the spatial distribution of the CCs calculated using daily precipitation data between the Seoul station and the remaining 59 stations. This provides an illustrative example of how the spatial similarities in terms of temporal coherence between two stations vary according to distance. For the observations, the CC decreases as the distance from the Seoul station increases. Majority of the stations located in the southern part of coastal region appear to be marginally related to the precipitation temporal evolution at the Seoul station. Similar to the observed pattern, all model simulations show a gradual decrease in the CCs with the distance. However, they behave differently in terms of the gradient in the decrease in the CCs. HAD_RAW shows consistently higher CCs than REG_RAW and WRF_RAW. Therefore, HAD_RAW still retains CC of at least 0.7 (yellow colour) around 36°N, which is more than 100 km from Seoul station. The critical deficiency of HAD_RAW can be found on the comparison between the Inje and Sokcho stations. The actual distance between the Inje and Sokcho stations is not that far; however, the precipitation pattern between them is quite different due to the effect of the geographical settings. The main ridge of the Taebaek Mountains stretching from north to south along the eastern coastal region lies between the Inje and Sokcho stations. As a result, Sokcho is located in the plain coastal region, whereas Inje is located further into the inland mountainous region (see Figure 1a). Because the representation of geographical settings largely depends on the model resolution, HAD_RAW, which has a coarse grid, is not able to accurately resolve the complex geography (e.g., topography and land–sea contrast), which may be the main reason for the failure to capture the region-specific characteristics of the observed pattern. More specifically, only HAD_RAW shows higher CCs of both the Sokcho (CC = 0.87) and Inje (CC = 0.94) stations than the observations and two downscaled

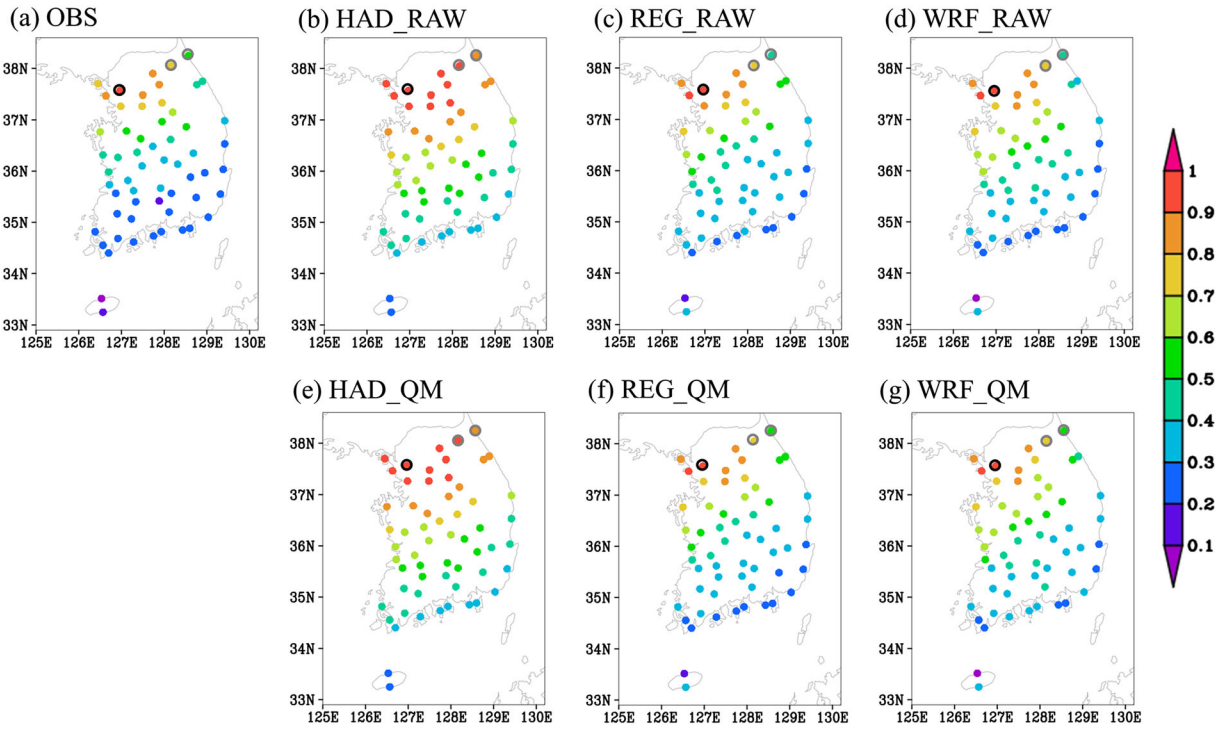

FIGURE 3 Spatial distributions of the temporal correlation coefficient for daily precipitation between the Seoul station and the other stations derived from the observations (a); raw outputs of HAD_RAW (b), REG_RAW (c), and WRF_RAW (d); and the bias-corrected outputs of HAD_QM (e), REG_QM (f), and WRF_QM (g). The point with the black line represents the Seoul station, and the two points with the grey line represent the Inje (inland) and Sokcho (coastal) stations

results. This result implies that HAD_RAW tends to produce precipitation at both Sokcho and Inje stations, which are highly correlated with that at the Seoul station. In contrast, REG_RAW and WRF_RAW produce much lower CCs in Sokcho than in Inje, which is closer to the observed pattern. However, whether this deficiency in the raw output can be improved using bias correction remains to be determined. Because climate model simulations are not completely accurate, the statistical bias-correction method is widely applied. In this study, we apply QM to the raw GCM (e.g., HAD_RAW) and raw RCMs (REG_RAW and WRF_RAW) to investigate the impact of bias correction on the spatial variability of precipitation. A comparison of the results with and without bias correction indicates that bias correction does not lead to any notable changes.

The aforementioned are more clearly revealed in Figure 4, which presents a scatterplot of the CCs of daily precipitation versus distance for all pairwise combinations of the 60 stations. The total number of combinations is 1,770 pairs. Consistent with the spatial pattern of the CCs in Figure 3, the spatial dependence of the observed daily precipitation decreases sharply with increasing distance, especially at a distance of less than 100 km. Focusing on this relatively short distance between paired data (e.g., less than 100 km), the well-defined pattern that differentiates the downscaled RCM results from the driving GCM can be found. The most notable difference appears in the decreasing gradient in the CCs. HAD_RAW retains CCs exceeding 0.8 of CCs until a distance of 100 km, which is not surprising considering the horizontal resolution employed in HAD_RAW. In contrast, REG_RAW and WRF_RAW are able to capture major characteristics of the decreasing in the CCs, which are similar to the observations, thus indicating the potential for improvements in simulating localized precipitation patterns. A narrow CC spread is another weakness of the HAD_RAW simulation. In the observations, the CCs show a large scatter ranging from 0.8 to 0.3 at a distance of 100 km, which indicates that the nature of precipitation over Korea is not simple or monotonic. Instead, the precipitation over South Korea is characterized by distinct seasonal and regional variability governed by different mechanisms (Im, In, & Han, 2013), which induce localized and synoptic-scale precipitation patterns on a case-by-case basis. By comparing the CC distribution that measures the relationship between precipitation and distance, both REG_RAW and WRF_RAW consistently show better agreement with the observed pattern than HAD_RAW. An important aspect for bias correction can be derived from the comparison of raw simulations and bias-corrected simulations. Identifying the relevant difference from simulations with and without bias correction is difficult. QM does not appear to be able to modulate the relationship in daily precipitation across stations. Although the statistical bias correction method (e.g., QM) can improve the climatological mean precipitation at individual locations (Lee, Lu, et al., 2019), it may not effectively adjust the occurrence of precipitation and the interstation relationship. This drawback will be further discussed in the next section.

On the basis of the different model performances in capturing the spatial variability of daily precipitation measured by the CCs for all pairwise combinations at the 60 stations over South Korea, we narrow the analysis to the Han River basin, where the hydrological simulation

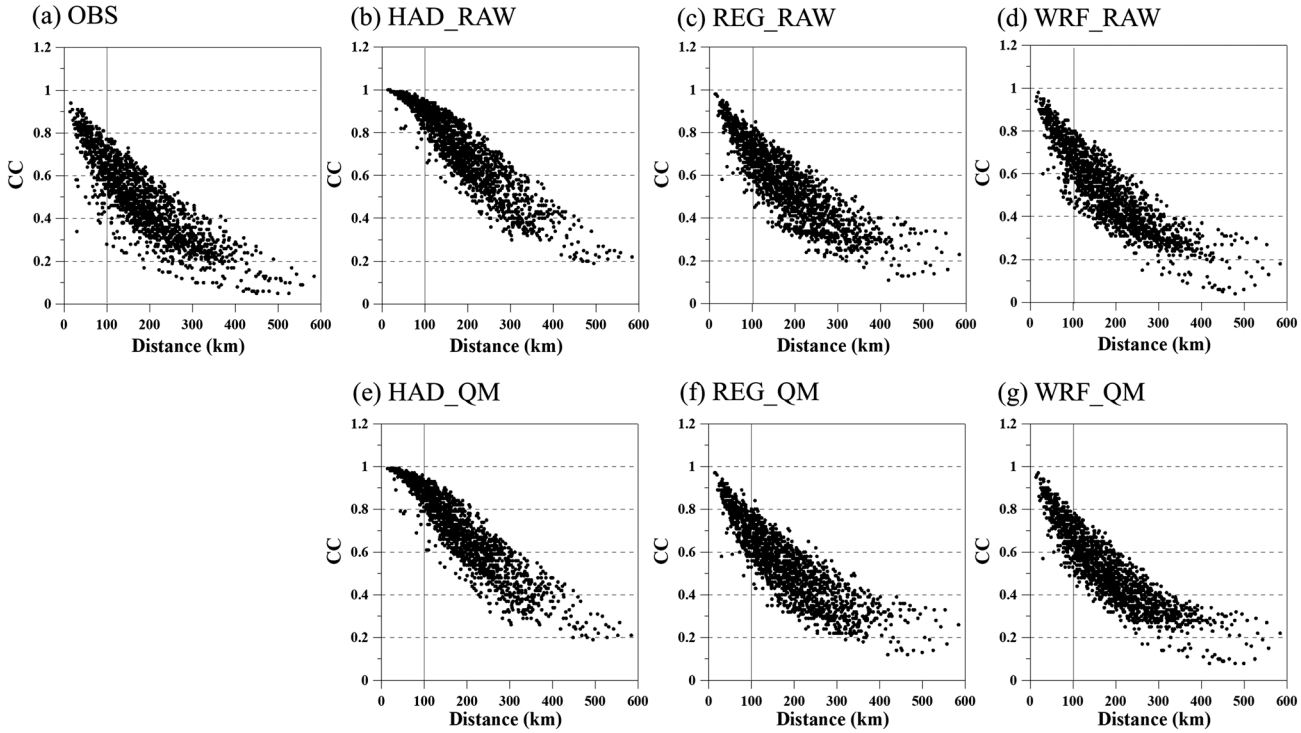

FIGURE 4 Scatterplot of the correlation coefficients for daily precipitation versus their interstation distances (60 stations, 1981–2005) derived from the observations (a); raw outputs of HAD_RAW (b), REG_RAW (c), and WRF_RAW (d); and the bias-corrected outputs of HAD_QM (e), REG_QM (f), and WRF_QM (g)

using the SWAT model is targeted. Figure 5 shows the empirical variance against distance and sill and range values determined by the weighted least squares method using the spherical variogram, which is calculated using the daily observed precipitation at 67 stations that are densely located in the Han River basin (see Figure 1b: weather stations plus rain gauges). We select four specific days that have distinctly different characteristics of precipitation in terms of the spatial distributions and amounts as presented in Figure 5. For example, the first case (1981.09.24) represents a high spatial variability of precipitation because the region with nonprecipitation and the region with high-intensity precipitation (e.g., more than 100 mm/day) are contiguous. In contrast, the fourth one (1981.07.01) represents a spatially less variable case because the Han River basin is mostly covered by intense precipitation. Such behaviours are well reflected in the slope of the variogram curve, which indicates that a steeper change rate of precipitation versus increment of distance leads to a shorter distance to reach the range value. More specifically, the range values for four cases are approximately 19, 46, 154, and 171 km. Because the range measures the distance at which two stations are unrelated, the range value decreases as the spatial variability increases. Moreover, the sill value is tied to the precipitation intensity because it refers to the variance corresponding to the distance of range. Because the variance is based on the squared quantity, the range varies substantially with the difference in the amount of precipitation between locations. For example, the first and fourth cases show larger sill values (i.e., 1,211 and 4,181 mm^2) because regions with very intense precipitation may lead to larger differences than regions with less precipitation, whereas the third case shows the smallest sill (i.e., 51 mm^2) because the maximum precipitation is less than 30 mm/day.

As indicated by the observed pattern in Figure 5, the range and sill values can be used as good descriptive statistics that describe the precipitation characteristics in a quantitative manner. Figures 6 and 7 present the frequency histograms of the range and sill attained from the variogram of daily precipitation over the Han River basin from the observations and six different model simulations. Among a total of 9,131 days (365 days × 25 years +6 days) during the 25-year historical period, the cases are included in the calculation of frequency when at least one subbasin has a daily precipitation amount greater than 1 mm. First, the entire frequency distribution of the range (Figure 6) from the observed daily precipitation provides the general precipitation spatial structures. Dominant precipitation patterns occupying more than 70% of the total precipitation over the Han River basin are characterized by large range values of more than 150 km, which correspond to the third and fourth cases in Figure 5c,d. This finding supports the notion that most precipitation events occur in broad regions, maintaining similarity across neighbouring basins. However, the less frequent precipitation cases with relatively smaller range values still account for a sizeable portion (approximately 20% for less than 100 km); thus, they should not be considered unimportant or trivial. Because we focus primarily on the cases representing high spatial variability over a short distance, the frequency distribution for the range value up to 110 km is enlarged and compared with the model simulations. In general, all simulations systematically underestimate the frequency of precipitation at small range values, particularly values

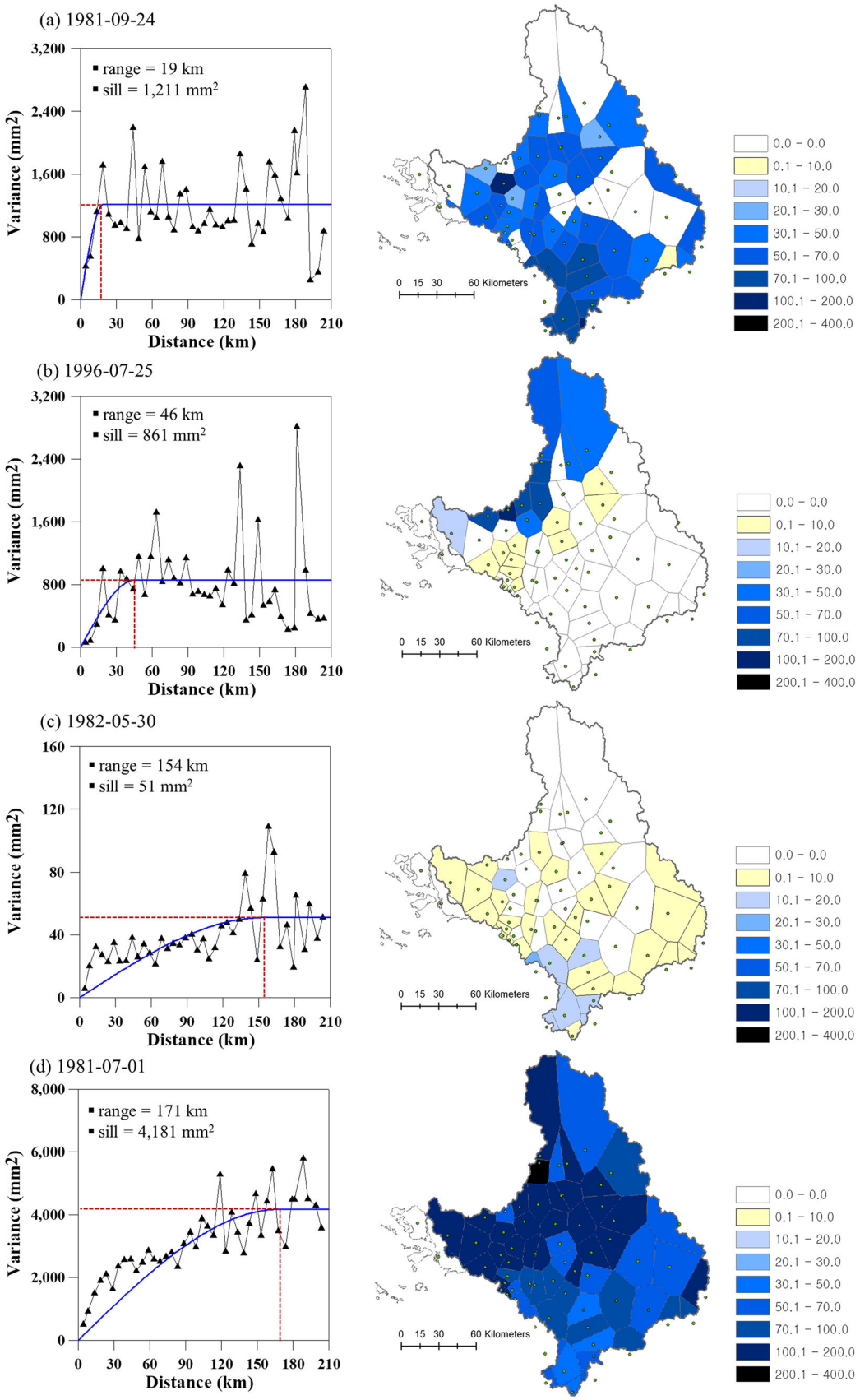

FIGURE 5 Examples of fitted variograms and spatial distribution of daily precipitation for four specific days with different ranges. The blue line is the fitted variogram, and the dotted red line represents the estimated sill and range. The Thiessen polygon method is used to interpolate the precipitation data from 67 stations

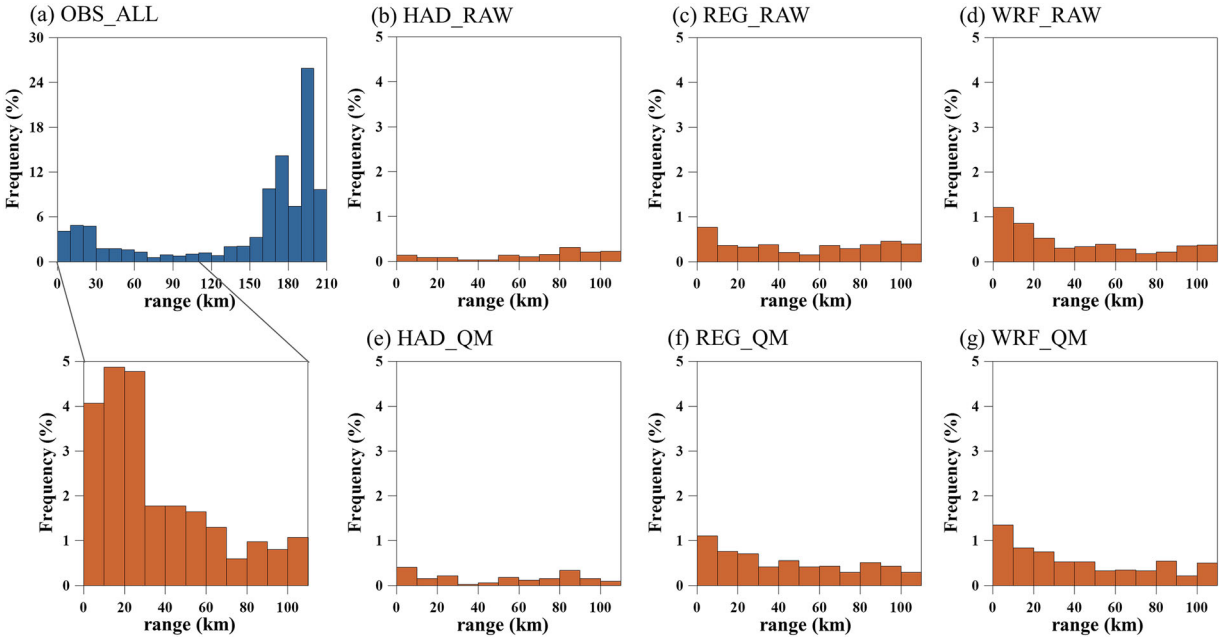

FIGURE 6 Histogram of the range (km) for daily precipitation over the historical period derived from observations (a); raw outputs of HAD_RAW (b), REG_RAW (c), and WRF_RAW (d); and bias-corrected outputs of HAD_QM (e), REG_QM (f), and WRF_QM (g). (a) shows the frequencies of all ranges (0–210 km), whereas the other figures show the frequencies within 100 km to clearly assess low range values

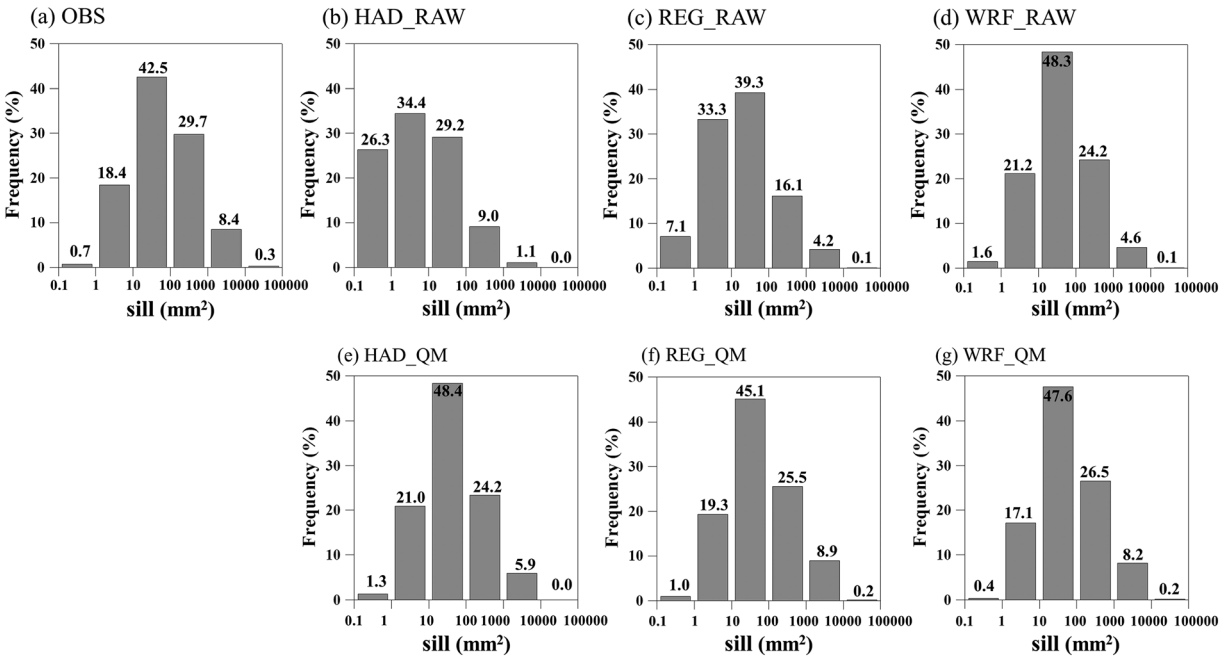

FIGURE 7 Histogram of sill (mm^2) for the daily precipitation over the historical period derived from observations (a); raw outputs of HAD_RAW (b), REG_RAW (c), and WRF_RAW (d); and bias-corrected outputs of HAD_QM (e), REG_QM (f), and WRF_QM (g)

less than 30 km. Whereas 14% of the observed daily precipitation amounts consist of the range values of 0–30 km, the precipitation amounts from HAD_RAW, REG_RAW, and WRF_RAW indicate a much lower portion in the same range, that is, 0.3%, 1.5%, and 2.3%, respectively. This deficiency in the raw output appears to be not significantly improved by applying the bias correction, which is consistent with the results of Figure 4. Although slight increases in the frequency are found for the range values of 0–30 km, they are very marginal improvements (i.e., 0.3% ➔ 0.8%, 1.5% ➔ 2.4%, and 2.3% ➔ 2.5%). The statistical bias correction using QM may not improve the model's original performance in capturing the proper coverage of localized precipitation that can critically affect the range.

Regarding the frequency distribution of the sill (Figure 7), the observed precipitation occurs most frequently in the range of 10 to 100 mm^2, which indicates relatively weak precipitation corresponding to the third case in Figure 5. A sill value of 1,000 mm^2 is roughly equivalent to the 45-mm difference in precipitation between station pairs, and this case means that a station receives at least 45 mm/day of precipitation when the paired station has no precipitation. The frequency of sill values greater than 1,000 mm^2 accounts for 8.7%, which includes the first and fourth cases in Figure 5. By comparison, notable differences are found in model performance between the RCMs (i.e., REG_RAW and WRF_RAW) and driving GCM (i.e., HAD_RAW). The REG_RAW and WRF_RAW reasonably simulate the sill characteristics for the relative ratios of the frequency by capturing not only the peak (between 10 and 100 mm^2) but also the upper and lower tails. In contrast, the frequency distribution from HAD_RAW is completely different from the observed one. Approximately 90% of the precipitation occurs for sill values less than 100 mm^2, which leads to a skewed distribution. In particular, very small sill values are unrealistically dominant, and the most frequent sill appears in the range of 1 to 10 mm^2. In addition, HAD_RAW shows a very low frequency of sill values over 1,000 mm^2. All of these limitations stem from the inability of HAD_RAW to capture intense precipitation. However, unlike the range, the bias correction leads to a significant improvement in the distribution of the sill. Compared with the different performances of the raw output, the broad pattern in the distribution of HAD_QM appears to be comparable with those from REG_QM and WRF_QM, which implies that QM results in a greater adjustment of the precipitation amount in HAD_QM than in REG_QM and WRF_QM. This result is quite different from that seen in the analysis of the range (Figure 6). Therefore, our study suggests that bias correction using QM presents different levels of effectiveness in adjusting the range and sill. Understanding the physical meaning of bias correction behind a large modification of precipitation amount and a slight modification in the spatial variability is essential for interpreting the hydrological response to different climate inputs (see Section 3.2).

3.2 | Impact of the spatial variability in precipitation on the hydrological simulations

In this section, hydrological simulations are mainly analysed to examine how the different performances of simulated precipitation can affect hydrological processes and how a large reduction in the bias for the present climate can affect future projections when assuming the existence of the same bias in the future. To accomplish these goals, the SWAT hydrological model is used with the 12 different climate input dataset, which are the raw and bias-corrected GCM (i.e., HAD_RAW and HAD_QM) and the raw and bias-corrected RCMs (i.e., REG_RAW, WRF_RAW, REG_QM, and WRF_QM) for the reference (1981–2005) and future (2076–2100) periods. We also perform SWAT simulations fed by observed meteorological data for the same period of the reference simulation. Note that because the reference simulation is not a reproduction experiment but a scenario experiment forced by historical GHG emissions, the SWAT simulation fed with the reference simulation cannot be compared with the SWAT simulation fed with observations based on a particular day and year. However, the SWAT simulation fed with observations can provide exemplary behaviour that helps identify limitations or problems arising from different climate input performances.

Figure 8 presents the annual maximum daily streamflow (AMDS) at the inlet of the Paldang Dam driven by observations, raw outputs, and bias-corrected outputs for the reference period. In this section, we avoid the analysis based on the long-term averaged climatology because the effect of spatial variability in precipitation on the hydrological simulation may be obscured. For the AMDS at the Paldang Dam simulated by SWAT with observations, a strong interannual variability is found. A majority of the year shows AMDS values in the range of 6,000–12,000 m^3/s, whereas for an abnormal year, the high and low flows reach approximately 29,000 m^3/s and 2,950 m^3/s, respectively. The AMDSs driven by HAD_RAW, REG_RAW, and WRF_RAW all severely underestimate the interannual variability because they fail to capture abnormally high peak flows, even though they show reasonable performance for low peak flow and 25-year average AMDS (OBS = 12,760 m^3/s, HAD_RAW = 9,870 m^3/s, REG_RAW = 10,910 m^3/s, and WRF_RAW = 11,500 m^3/s). Interestingly, the AMDS driven by the bias-corrected precipitation shows a very different response between the RCMs and the driving GCM. The AMDS driven by HAD_QM exceeds 30,000 m^3/s three times, although this value has never been observed for AMDS driven by measured dam inflow, and the maximum is 36,120 m^3/s. Unrealistically high AMDS values tend to occur with an additional problem in which lower AMDSs are increased to much higher values; otherwise, an appropriate range of lower AMDSs driven by HAD_RAW is observed. However, the dramatic change obtained with HAD_QM-led AMDS is not found in the AMDS driven by REG_QM and WRF_QM. For the AMDS patterns from the RCMs, bias-corrected precipitation may play a role in enhancing the AMDS for the abnormally high peak year, although the general phase of the annual AMDS fluctuations and the range of lower AMDS values are preserved.

To reveal the key factor underlying the different impacts of bias-corrected precipitation on streamflow simulations driven by RCMs and GCM, we compare the spatial distribution of runoff driven by raw and bias-corrected precipitation from August 24 to 26, 1989 (Figure 9). This period is targeted because the AMDS driven HAD_QM produces an extremely high value for August 26, 1989 (see Figure 8b). The runoff averaged over the Han River basin driven by HAD_RAW is not substantially different from those of REG_RAW and WRF_RAW, although they show quite different spatial variability and 3-day evolutionary patterns of runoff. The differences in the runoff spatial and temporal patterns are much more amplified when fed by bias-corrected precipitation, which in turn leads to dramatic differences in streamflow. More specifically, runoffs driven by HAD_QM and REG_QM largely increase compared with those from HAD_RAW and REG_RAW, and their basin-averaged values are 248 and 236 mm, respectively, during August 25 and 26. Despite the qualitatively similar amount of runoff, the streamflow has a large difference of

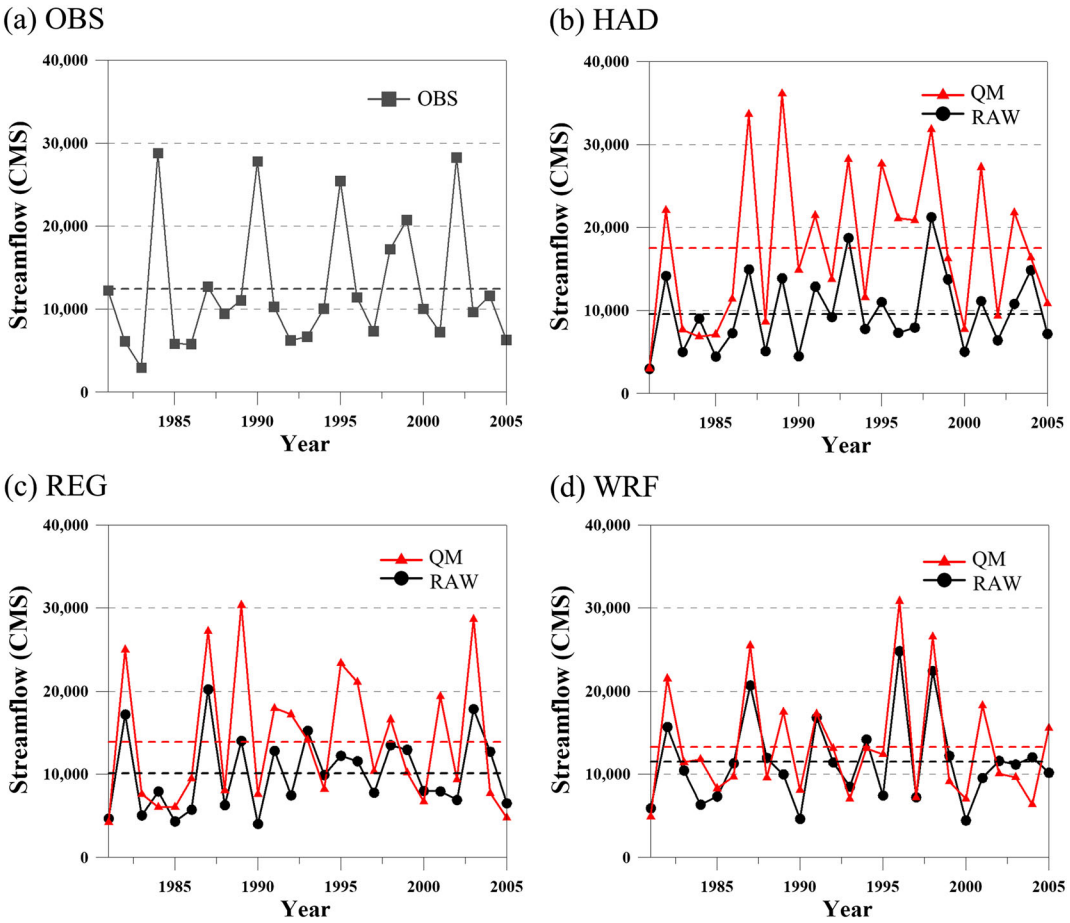

FIGURE 8 Annual maximum daily streamflow at outlets of the Paldang Dam driven by observation (a), raw outputs, and bias corrected outputs. Black and red lines indicate AMDSs derived from the raw outputs and the bias-corrected outputs, respectively. The dashed line represents the average value for each case

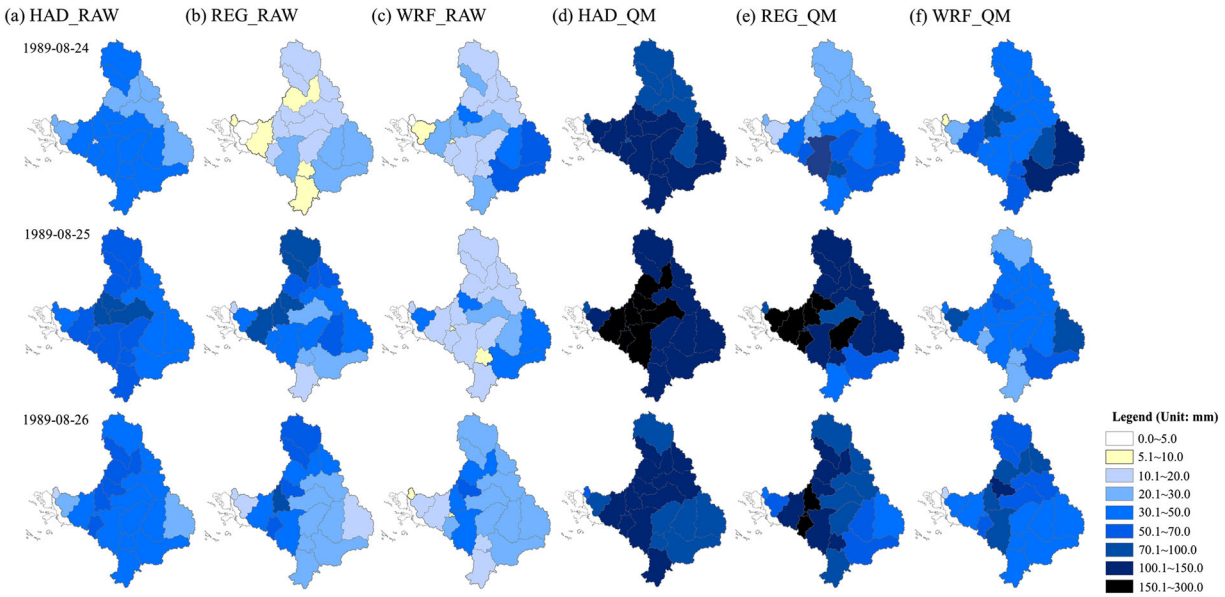

FIGURE 9 Spatial distribution of runoff obtained from the raw outputs (HAD_RAW, REG_RAW, and WRF_RAW) and the bias-corrected outputs (HAD_QM, REG_QM, and WRF_QM) in the Han River basin from August 24 to 26, 1989

approximately 6,000 m^3/s between HAD_QM and REG_QM for August 26. The key determinant behind the marked difference in the streamflow pattern is the spatial variability of runoff. Whereas REG_QM exhibits locally intensified runoff that is restricted with a certain area, HAD_QM produces intensified runoff with a large coverage due to the lack of spatial variability. Therefore, the convergence caused by strong runoff encompassing the large faction of the basin immediately renders the peak flows at the inlet of the Paldang Dam.

To demonstrate whether the runoff pattern driven by RCM-based precipitation is more realistic than that driven by the GCM, we analyse the spatial distribution of runoff simulated by the observed meteorological data for three events (Figure 10). September 2, 1984; September 11, 1990; and August 7, 2002, are selected for the high streamflow occurrence, and 2 days before peak date are also included in the analysis (Figure 10). Although a direct comparison between this and the result in Figure 9 is not permitted, this analysis can serve as a proxy for understanding the typical behaviour of observed runoff. All three cases are characterized by distinct spatial and temporal variability. The region with maximum runoff varies at the daily timescale according to the evolution of precipitation, and the spatial patterns resemble a collection of small patches. These behaviours in runoff are much closer to those driven by RCM-based precipitation seen in Figure 9.

Problems with the runoff pattern that directly respond to precipitation will affect the streamflow. Because the same bias correction factors derived from the reference simulations are applied to the future projections, it is important to compare the precipitation and resultant streamflow from the raw and bias-corrected output for the future period. Figure 11 presents the daily streamflow hydrograph and precipitation for September 2085 because this month includes one of the highest streamflow events, which occurs on September 10, for all hydrological simulations driven by HAD_QM, REG_QM, and WRF_QM. To obtain a better understanding of the effect on the dispersion and basin lag when forming the peak flow, we investigate the streamflow and precipitation averaged over the Paldang Dam basin as well as the Soyanggang Dam and Chungju Dam basins, which are located in the upstream basin of the Paldang Dam (see Figure 1 for their locations). Regardless of the basins, the most distinct pattern appearing in the bias-corrected GCM is a significant increase in precipitation and resultant streamflow compared with the raw output. The precipitation amounts averaged over the Paldang Dam basin from HAD_RAW and HAD_QM are 302 and 689 mm from September 7 to 12. The corrected precipitation rate is 2.3 times higher, and this provides a peak flow that is roughly 3.0 times higher, resulting in unrealistic streamflow of 38,770 m^3/s from HAD_QM. However, the corrected rates of precipitation from REG_QM and WRF_QM are

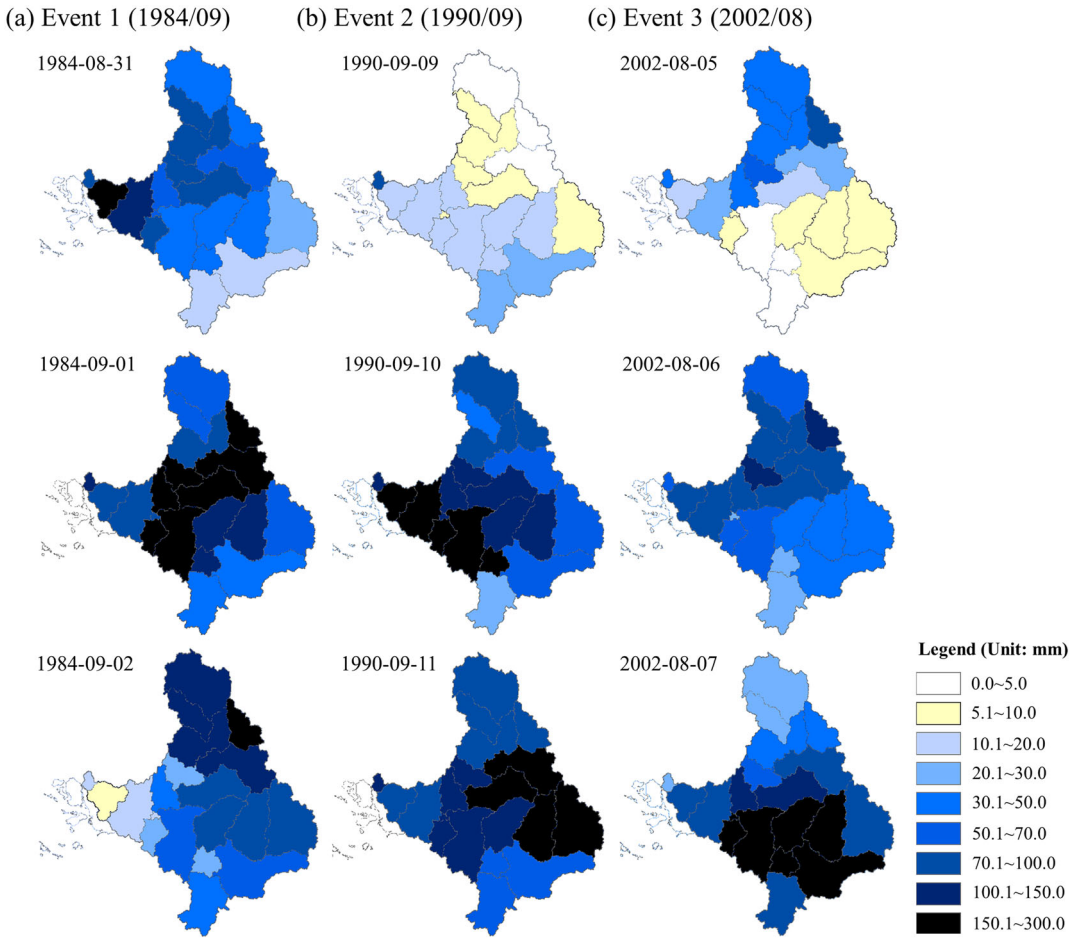

FIGURE 10 Spatial distribution of runoff simulated using observed climate data in the Han River basin for three events with high streamflows

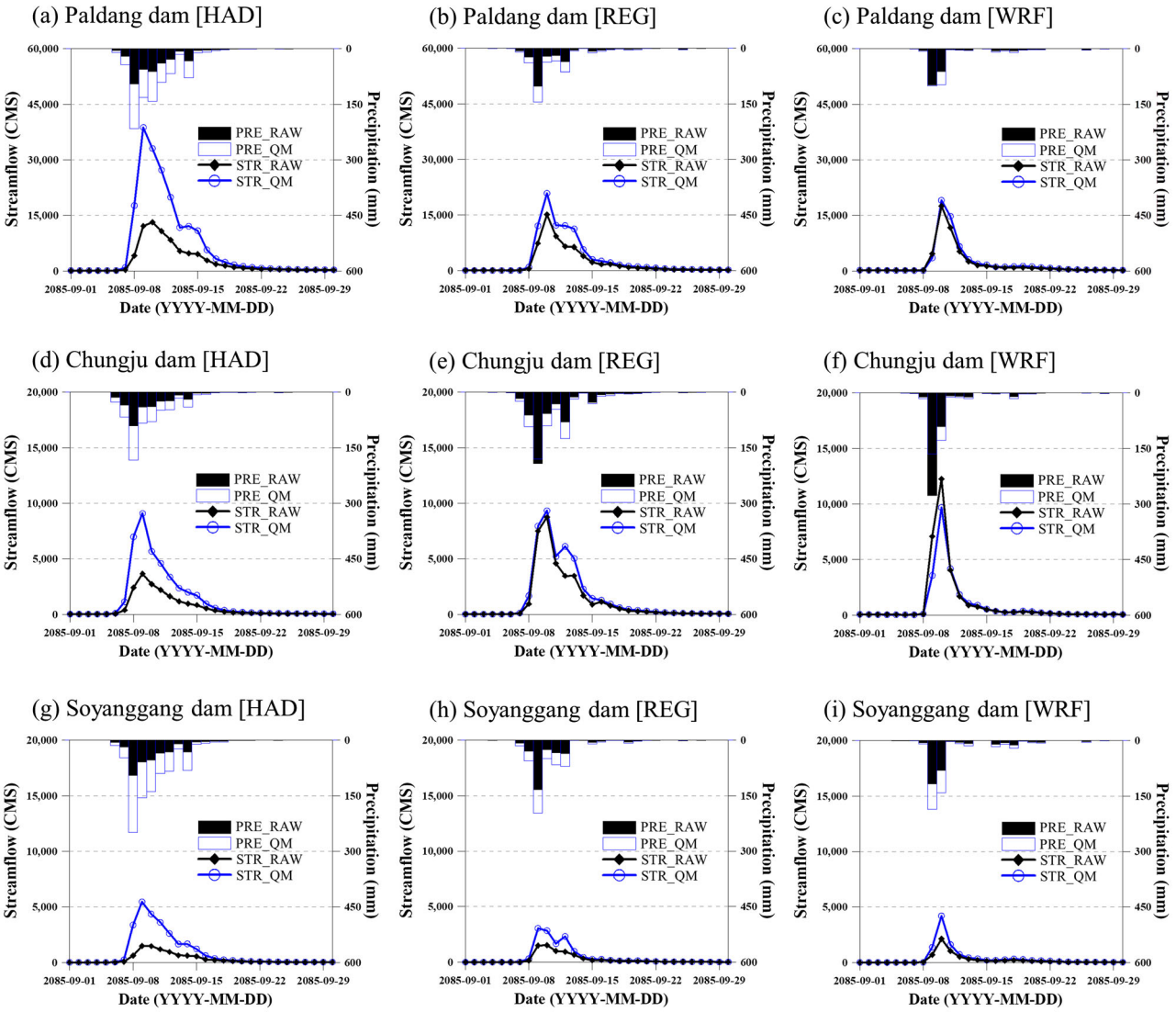

FIGURE 11 Time series of daily streamflow at the inlets of the Paldang Dam, Chungju Dam, and Soyanggang Dam and the mean areal daily precipitation at the Paldang Dam, Chungju Dam, and Soyanggang Dam basins from September 1 to 30, 2085. Blue and black lines indicate streamflow derived from the raw outputs and the bias-corrected outputs, respectively. Blue and black bars indicate the mean areal precipitation derived from the raw outputs and the bias-corrected outputs, respectively

approximately 1.6 and 1.2 times, which subsequently leads to increases in the peak flow of approximately 1.4 and 1.1 times, respectively. Therefore, the peak flows driven by the bias-corrected output are completely different among HAD_QM (38,770 m^3/s), REG_QM (20,840 m^3/s), and WRF_QM (19,060 m^3/s), although HAD_RAW, REG_RAW, and WRF_RAW produce similar values.

The distinctly different responses between the bias-corrected GCM and bias-corrected RCMs can be partly explained by Figure 12 , which shows the spatial distribution of runoff from September 8 to 11, 2085. The spatial distribution of runoff driven by HAD_RAW is quite different from that of REG_RAW and WRF_RAW. Whereas the spatial variability of runoff driven by RCM-based precipitation primarily comprises both very low and very high values, the runoff driven by HAD_RAW shows a different behaviour exhibiting similar values across most of the basin. The highest runoff driven by HAD_RAW occurs near the Paldang Dam, and the runoff amount decreases slowly in the upper basins. In contrast, the RCM-based runoff is highest in the Chungju and Soyanggang basins, which is because the precipitation from HAD_RAW is affected by one GCM grid point, which is near the Paldang Dam (see GCM grid points in Figure 1), whereas the RCM-based precipitation is generated by considering the spatial variations of detailed topographical and meteorological characteristics such as mountainous effect and wind fields. After the bias correction, the characteristics of the spatial variability do not change significantly, although a large increase in runoff is found in all simulations. Because HAD_RAW fails to capture the spatially distinct pattern of runoff, the increase in precipitation in HAD_QM does not occur locally. Consequently, the streamflow feeding HAD_QM results in unrealistically high flows that are converged by broadly intensified runoff.

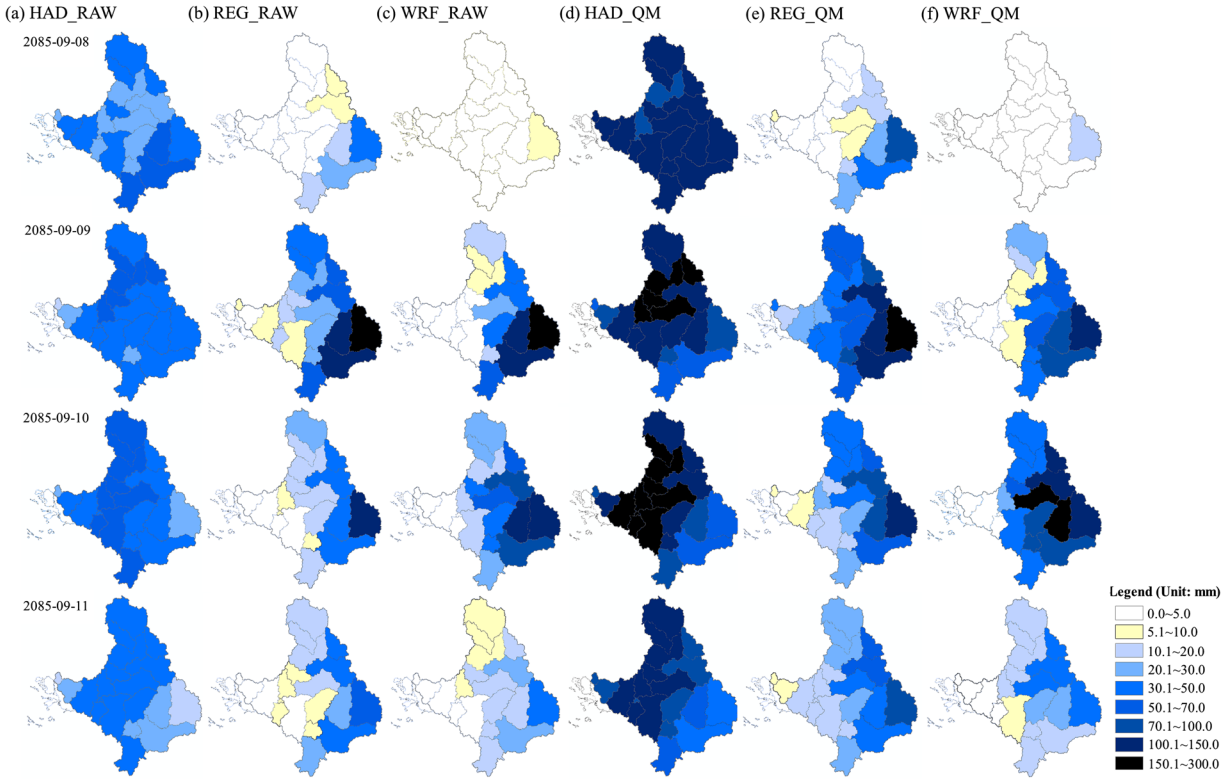

FIGURE 12 Spatial distribution of runoff obtained by the raw outputs (HAD_RAW, REG_RAW, and WRF_RAW) and the bias-corrected outputs (HAD_QM, REG_QM, and WRF_QM) in the Han River basin from September 8 to 11, 2085

4 | SUMMARY AND CONCLUSIONS

The spatial variability of precipitation is a critical factor for simulating streamflow. It is generally regarded that RCMs exhibit relatively better performance than GCMs in terms of capturing the spatial variability of precipitation because the horizontal resolution of RCMs is much higher than that of GCM. Nevertheless, the effectiveness of dynamical downscaling using RCMs is still a subject of controversy when linking climate simulations with hydrological models.

In this study, we investigate the added value of dynamic downscaling on hydrological projections in terms of the spatial variability of precipitation. To set up the input data for a semidistributed hydrological model (SWAT), the GCM projection (HadGEM) is downscaled by either a simple disaggregation or two RCMs (RegCM and WRF), and statistical bias correction using the QM method is then applied to the daily output derived from the GCM and two RCMs. The comparative analysis of precipitation characteristics from the raw and bias-corrected output clearly reveals the limitation and effectiveness of statistical bias correction. Our study suggests that bias correction using QM presents different levels of performance in improving the precipitation intensity and its spatial variability, which leads to a quite different hydrological behaviour in response to GCM- and RCM-based precipitation. The spatial variability of daily precipitation does not change significantly after applying bias correction, emphasizing the importance of the performance of the raw output. By comparing with the precipitation from GCM, the statistics derived from RCM-based precipitation are much closer to those of the observations, in which the spatial autocorrelation is sharply decreased within a relatively short distance. In contrast to spatial variability, a significant reduction in the bias related to the precipitation intensity is commonly found in both the GCM and RCMs simulations when applying bias correction. However, the large bias correction factor that is required to compensate for the large discrepancy in the reference simulation against the observations may cause a serious distortion in the raw output, particularly when the raw output is too coarse to represent the local variability. Such a problem tends to be amplified in the future projection. For example, if the severely underestimated precipitation from GCM raw output is intensified several times through the bias correction without considering the localized spatial variability, the future precipitation is largely intensified by the same correction factor across the entire basin, which in turn exaggerates the runoff. The deficiency seen in the precipitation and runoff spatial patterns is directly transferred to the shape of the streamflow hydrographs, leading to unrealistically high flows. However, the RCM-based streamflows show reasonable performance in both qualitative (e.g., spatial distribution) and quantitative (e.g., peak flow magnitude) aspects. Furthermore, the discrepancy in the peak flows driven by the raw and bias-corrected precipitation is much smaller in the RCMs than in the GCM, which is important to enhance the reliability of hydrological extremes in the context of future projection.

ACKNOWLEDGMENTS

This work is supported by the Korea Environmental Industry & Technology Institute (KEITI) grant funded by the Ministry of Environment

(Grant RE201901084). We thank Prof. Joong-Bae Ahn and Dr Yeon-Woo Choi at Pusan National University for providing WRF projections driven by HadGEM2-AO. We also extend our thanks to Prof. Myoung-Seok Suh and Dr Seok-Geun Oh at Kongju National University for providing the RegCM4 projections driven by HadGEM2-AO.

DATA AVAILABILITY STATEMENT

Daily observed weather and dam inflow data used in this study can be found in the Water Resources Management Information System (http://www.wamis.go.kr/eng/main.aspx#), which are publicly available. Model-driven datasets used in this study are available from the corresponding author, upon reasonable request.

ORCID

Moon-Hwan Lee https://orcid.org/0000-0002-5445-9808
Eun-Soon Im https://orcid.org/0000-0002-8953-7538
Deg-Hyo Bae https://orcid.org/0000-0002-0429-1154

REFERENCES

Ahmed, K. F., Wang, G., Silander, J., Wilson, A. M., Allen, J. M., Horton, R., & Anyah, R. (2013). Statistical downscaling and bias correction of climate model outputs for climate change impact assessment in the U.S. northeast. *Global and Planetary Change*, *100*, 320–332. https://doi.org/10.1016/j.gloplacha.2012.11.003

Ahn, J. B., Jo, S., Suh, M. S., Cha, D. H., Lee, D. K., Hong, S. Y., … Shim, K. M. (2016). Changes of precipitation extremes over South Korea projected by the 5 RCMs under RCP scenarios. *Asia-Pacific Journal of Atmospheric Sciences*, *52*, 223–236. https://doi.org/10.1007/s13143-016-0021-0

Arnold, J. G., Srinivasan, R., Muttiah, R. S., & Williams, J. R. (1998). Large area hydrologic modeling and assessment. Part I: Model development. *Journal of the American Water Resources Association*, *34*, 73–89. https://doi.org/10.1111/j.1752-1688.1998.tb05961.x

Bae, D. H., Jung, I. W., & Lettenmaier, D. P. (2011). Hydrologic uncertainties in climate change from IPCC AR4 GCM simulations of the Chungju basin, Korea. *Journal of Hydrology*, *401*, 90–105. https://doi.org/10.1016/j.jhydrol.2011.02.012

Baek, H. J., Lee, J., Lee, H. S., Hyun, Y. K., Cho, C. H., Kwon, W. T., … Kim, M. J. (2013). Climate change in the 21st century simulated by HadGEM2-AO under representative concentration pathways. *Asia-Pacific Journal of Atmospheric Sciences*, *49*(5), 603–618. https://doi.org/10.1007/s13143-013-0053-7

Baigorria, G. A., Jones, J. W., & O'Brien, J. J. (2007). Understanding rainfall spatial variability in southeast USA at different timescales. *International Journal of Climatology*, *27*, 749–760. https://doi.org/10.1002/joc.1435

Berndtsson, R. (1988). Temporal variability in spatial correlation of daily rainfall. *Water Resources Research*, *24*, 1511–1517. https://doi.org/10.1029/WR024i009p01511

Beven, K. J., & Hornberger, G. M. (1982). Assessing the effect of spatial pattern of precipitation in modeling stream flow hydrographs. *Journal of the American Water Resources Association*, *18*(5), 823–829. https://doi.org/10.1111/j.1752-1688.1982.tb00078.x

Chang, H., & Jung, I. W. (2010). Spatial and temporal changes in runoff caused by climate change in a complex large river basin in Oregon. *Journal of Hydrology*, *388*, 186–207. https://doi.org/10.1016/j.jhydrol.2010.04.040

Collins, W. J., Bellouin, N., Doutriaux-Boucher, M., Gedney, N., Halloran, P., Hinton, T., … Woodward, S. (2011). Development and evaluation of an Earth-System model HadGEM2. *Geoscientific Model Development*, *4*, 1051–1075. https://doi.org/10.5194/gmd-4-1051-2011

Coppola, E., Raffaele, F., & Giorgi, F. (2018). Impact of climate change on runoff timing over the Alpine region. *Climate Dynamics*, *51*(3), 1259–1273. https://doi.org/10.1007/s00382-016-3331-0

Cressie, N. A. (1985). Fitting variogram models by weighted least squares. *Journal of the International Association for Mathematical Geology*, *17*, 563–586. https://doi.org/10.1007/BF01032109

Cressie, N. A. (1993). *Statistics for spatial data*. NY: Wiley. revised edn

Cristiano, E., ten Veldhuis, M. C., & van de Giesen, N. (2017). Spatial and temporal variability of rainfall and their effects on hydrological response in urban areas- a review. *Hydrology and Earth System Sciences*, *21*, 3859–3878. https://doi.org/10.5194/hess-21-3859-2017

Cunge, J. A. (1969). On the subject of a flood propagation computation method (Muskingum method). *Journal of Hydraulic Research*, *7*, 205–230. https://doi.org/10.1080/00221686909500264

Dosio, A., & Paruolo, P. (2011). Bias correction of the ENSEMBLES high-resolution climate change projections for use by impact models: Evaluation on the present climate. *Journal of Geophysical Research*, *116*, D16106. https://doi.org/10.1029/2011JD015934

Eden, J. M., Widmann, M., Maraun, D., & Vrac, M. (2014). Comparison of GCM- and RCM- simulated precipitation following stochastic postprocessing. *Journal of Geophysical Research-Atmospheres*, *119*, 11040–11053. https://doi.org/10.1002/2014JD021732

Giorgi, F., Coppola, E., & Raffaele, F. (2014). A consistent picture of the hydroclimatic response to global warming from multiple indices: Models and observations. *Journal of Geophysical Research*, *119*, 11695–11708.

Giorgi, F., Coppola, E., Solmon, F., Mariotti, L., Sylla, M. B., Bi, X., … Brankovic, C. (2012). RegCM4: Model description and preliminary tests over multiple CORDEX domains. *Climate Research*, *52*, 7–29. https://doi.org/10.3354/cr01018

Habib, E., Krajewski, W. F., & Ciach, G. J. (2001). Estimation of rainfall interstation correlation. *Journal of Hydrometeorology*, *2*, 621–629. https://doi.org/10.1175/1525-7541(2001)002<0621:EORIC>2.0.CO;2

Henn, B., Clark, M. P., Kavetski, D., Newman, A. J., Hughes, M., McGurk, B., & Lundquist, J. D. (2018). Spatiotemporal patterns of precipitation inferred from streamflow observations across the Sierra Nevada mountain range. *Journal of Hydrology*, *556*, 993–1021. https://doi.org/10.1016/j.jhydrol.2016.08.009

Im, E. S., Ahn, J. B., & Jo, S. R. (2015). Regional climate projection over South Korea simulated by the HadGEM2-AO and WRF model chain under RCP emission scenarios. *Climate Research*, *63*, 246–266.

Im, E. S., & Eltahir, E. A. B. (2018). Simulation of the diurnal variation of rainfall over the western Maritime Continent using a regional climate model. *Climate Dynamics*, *51*, 73–88. https://doi.org/10.1007/s00382-017-3907-3

Im, E. S., In, S. R., & Han, S. O. (2013). Numerical simulation of the heavy rainfall caused by a convection band over Korea: A case study on the comparison of WRF and CReSS. *Nature Hazards*, *69*, 1681–1695. https://doi.org/10.1007/s11069-013-0779-7

Im, E. S., Kwon, W. T., Ahn, J. B., & Giorgi, F. (2007). Multi-decadal scenario simulation over Korea using a one-way double-nested regional climate model system. Part I: Recent climate simulation (1971-2000). *Climate Dynamics*, *28*, 759–780. https://doi.org/10.1007/s00382-006-0203-z

IPCC (2013) Climate change 2013: The physical science basis. Contribution of working group i to the fifth assessment report of the

intergovernmental panel on climate change [Stocker, T.F., D. Qin, G.-K. Plattner, M. Tignor, S.K. Allen, J. Boschung, A. Nauels, Y. Xia, V. Bex and P.M. Midgley (eds.)]. Cambridge University Press, Cambridge, United Kingdom and New York, NY, USA, 1535 pp.

Jung, I. W., Bae, D. H., & Lee, B. J. (2013). Possible change in Korean streamflow seasonality based on multi-model climate projections. *Hydrological Processes*, *27*, 1033–1045. https://doi.org/10.1002/hyp.9215

Kokkonen, T., Koivusalo, H., Karvonen, T., & Croke, B. (2004). Exploring streamflow response to effective rainfall across event magnitude scale. *Hydrological Processes*, *18*, 1467–1486. https://doi.org/10.1002/hyp.1423

Korea Meteorological Administration (2015). Production of fine-scale climate change data over the Korean peninsula using RCP scenarios. Research Report (CATER 2012–3080), 822.

Lafon, T., Dadson, S., Buys, G., & Prudhomme, C. (2013). Bias correction of daily precipitation simulated by a regional climate model: A comparison of methods. *International Journal of Climatology*, *33*, 1367–1381. https://doi.org/10.1002/joc.3518

Lee, M. H., & Bae, D. H. (2018). Uncertainty assessment of future projections on water resources according to climate downscaling and hydrological models. *Journal of Hydroinformatics*, *20*, 597–607. https://doi.org/10.2166/hydro.2018.132

Lee, M. H., Im, E. S., & Bae, D. H. (2019). A comparative assessment of climate change impact on drought over Korea based on multiple climate projections and multiple drought indices. *Climate Dynamics*, 1–16. https://doi.org/10.1007/s00382-018-4588-2

Lee, M. H., Lu, M., Im, E. S., & Bae, D. H. (2019). Added value of dynamical downscaling for hydrological projections in the Chungju basin, Korea. *International Journal of Climatology*, *39*(1), 516–531. https://doi.org/10.1002/joc.5825

Ly, S., Charles, C., & Degre, A. (2011). Geostatistical interpolation of daily rainfall at catchment scale: The use of several variogram models in the Ourthe and Ambleve catchments, Belgium. *Hydrology and Earth System Sciences*, *15*, 2259–2274. https://doi.org/10.5194/hess-15-2259-2011

Maurer, E. P., & Pierce, D. W. (2014). Bias correction can modify climate model-simulated precipitation changes without adverse affect on the ensemble mean. *Hydrology and Earth System Sciences*, *18*, 915–925. https://doi.org/10.5194/hess-18-915-2014

Merino, G. G., Jones, D., Stooksbury, D. E., & Hubbard, K. G. (2001). Determination of semivariogram models to Krige hourly and daily solar irradiance in Western Nebraska. *Journal of Applied Meteorology and Climatology*, *40*, 1085–1094. https://doi.org/10.1175/1520-0450(2001)040<1085:DOSMTK>2.0.CO;2

Merz, B., & Bardossy, A. (1998). Effects of spatial variability on the rainfall runoff process in a small loess catchment. *Journal of Hydrology*, *212-213*, 304–317. https://doi.org/10.1016/S0022-1694(98)00213-3

Ngai, S. T., Tangang, F., & Juneng, L. (2017). Bias correction of global and regional simulated daily precipitation and surface mean temperature over Southeast Asia using quantile mapping method. *Global and Planetary Change*, *149*, 79–90. https://doi.org/10.1016/j.gloplacha.2016.12.009

Oh, S. G., & Suh, M. S. (2018). Changes in seasonal and diurnal precipitation types during summer over South Korea in the late twenty-first century (2081–2100) projected by the RegCM4.0 based on four RCP scenarios. *Climate Dynamics*, *51*, 3041–3060. https://doi.org/10.1007/s00382-017-4063-5

Oh, S. G., Suh, M. S., Lee, Y. S., Ahn, J. B., Cha, D. H., Lee, D. K., … Kang, H. S. (2016). Projections of high resolution climate changes for South Korea using multiple-regional climate models based on four RCP scenarios. Part 2: precipitation. *Asia-Pacific Journal of Atmospheric Sciences*, *52*, 171–189. https://doi.org/10.1007/s13143-016-0018-8

Shrestha, R. R., Schnorbus, M. A., Werner, A. T., & Zwiers, F. W. (2014). Evaluating hydroclimatic change signals from statistically and dynamically downscaled GCMs and hydrologic models. *Journal of Hydrometeorology*, *15*, 844–860. https://doi.org/10.1175/JHM-D-13-030.1

Singh, V. P. (1987). Effect of spatial and temporal variability in rainfall and watershed characteristics on stream flow hydrograph. *Hydrological Processes*, *11*, 1649–1669.

Skamarock, W. C., Klemp, J. B., Dudhia, J., Gill, D. O., Baker, D. M., Huang, X. Y., … Powers, J. G. (2008). *A description of the Advanced Research WRF version 3. NCAR Tech Note NCAR/TN-475+STR*. Boulder, CO: National Center for Atmospheric Research.

Smith, M. B., Koren, V. I., Zhang, Z., Reed, S. M., Pan, J. J., & Moreda, F. (2004). Runoff response to spatial variability in precipitation: An analysis of observed data. *Journal of Hydrology*, *298*, 267–286. https://doi.org/10.1016/j.jhydrol.2004.03.039

Suh, M. S., Oh, S. G., Lee, Y. S., Ahn, J. B., Cha, D. H., Lee, D. K., … Kang, H. S. (2016). Projections of high resolution climate changes for South Korea using multiple-regional climate models based on four RCP scenarios. Part 1: Surface air temperature. *Asia-Pacific Journal of Atmospheric Sciences*, *52*, 151–169. https://doi.org/10.1007/s13143-016-0017-9

Taylor, K. E., Stouffer, R. J., & Meehl, G. A. (2012). An overview of CMIP5 and the experiment design. *Bulletin of the American Meteorological Society*, *93*, 485–498. https://doi.org/10.1175/BAMS-D-11-00094.1

Teng, J., Potter, N. J., Chiew, F. H. S., Zhang, L., Wang, B., Vaze, J., & Evans, J. P. (2015). How does bias correction of regional climate model precipitation affect modelled runoff? *Hydrology and Earth System Sciences*, *19*, 711–728. https://doi.org/10.5194/hess-19-711-2015

Teutschbein, C., & Seibert, J. (2012). Bias correction of regional climate model simulations for hydrological climate-change impact studies: Review and evaluation of different methods. *Journal of Hydrology*, *456*, 12–29.

Torma, C., Giorgi, F., & Coppola, E. (2015). Added value of regional climate modeling over areas characterized by complex terrain-Precipitation over the Alps. *Journal of Geophysical Research-Atmospheres*, *120*, 3957–3972. https://doi.org/10.1002/2014JD022781

Trenberth, K. E., Dai, A., Rasmussen, R. M., & Parsons, D. B. (2003). The changing character of precipitation. *Bulletin of the American Meteorological Society*, *84*, 1205–1217. https://doi.org/10.1175/BAMS-84-9-1205

Tselioudis, G., Douvisa, C., & Zerefos, C. (2012). Does dynamical downscaling introduce novel information in climate model simulations of precipitation change over a complex topography region? *International Journal of Climatology*, *32*, 1572–1578. https://doi.org/10.1002/joc.2360

van de Beek, C. Z., Leijnse, H., Torfs, P. J. J. F., & Uijlenhoet, R. (2011). Climatology of daily rainfall semi-variance in the Netherlands. *Hydrology and Earth System Sciences*, *15*, 171–183. https://doi.org/10.5194/hess-15-171-2011

Vrac, M., & Friederichs, P. (2015). Multivariate-intervariable, spatial, and temporal-bias correction. *Journal of Climate*, *28*, 218–237. https://doi.org/10.1175/JCLI-D-14-00059.1

Xu, J., Chen, Y., Li, W., Liu, Z., Tang, J., & Wei, C. (2016). Understanding temporal and spatial complexity of precipitation distribution in Xinjiang, China. *Theoretical and Applied Climatology*, *123*, 321–333. https://doi.org/10.1007/s00704-014-1364-z

Zhang, L., Karthikeyan, R., Bai, Z., & Wang, J. (2017). Spatial and temporal variability of temperature, precipitation, and streamflow in upper Sang-

kan basin, China. *Hydrological Processes*, *31*, 279–295. https://doi.org/10.1002/hyp.10983

Zhou, F., Xu, Y., Chen, Y., Xu, C. Y., Gao, Y., & Du, J. (2013). Hydrological response to urbanization at different spatio-temporal scales simulated by coupling of CLUE-S and the SWAT model in the Yangtze River Delta region. *Journal of Hydrology*, *485*, 113–125. https://doi.org/10.1016/j.jhydrol.2012.12.040

How to cite this article: Lee M-H, Im E-S, Bae D-H. Impact of the spatial variability of daily precipitation on hydrological projections: A comparison of GCM- and RCM-driven cases in the Han River basin, Korea. *Hydrological Processes*. 2019;1–18. https://doi.org/10.1002/hyp.13469